

Thermoelectric efficiency of quantum dot molecules at a high temperature bias: the role of thermal-induced voltage

Chih-Chieh Chen[†]

*Research Center for Applied Sciences, Academic Sinica, Taipei, 11529 Taiwan and
Department of Physics, University of Illinois at Urbana-Champaign, Urbana, Illinois 6180, USA*

David M T Kuo^{††}

*Department of Electrical Engineering and Department of Physics,
National Central University, Chungli, 320 Taiwan*

Yia-Chung Chang^{*}

*Research Center for Applied Sciences, Academic Sinica, Taipei, 11529 Taiwan and
Department of Physics, National Cheng Kung University, Tainan, 701 Taiwan*

(Dated: November 6, 2018)

The nonlinear electron and heat currents of quantum dot molecules (QDMs) under a temperature bias are theoretically investigated, including all correlation functions arising from electron Coulomb interactions in QDMs. Unlike the case of double QDs, the maximum efficiency of serially coupled triple QDs (SCTQD) occurs in the orbital depletion regime owing to the interdot Coulomb blockade. The electron current in SCTQD shows a bipolar oscillatory behavior with respect to the variation of QD energy levels, whereas the heat current does not show such a behavior. This is mainly attributed to thermal-induced bias. In addition, we illustrate how the efficiency of SCTQD is influenced by the external load resistance, and phonon heat flow. Finally, a direction-dependent electron current driven by a temperature bias has been demonstrated for a SCTQD with staircase-like energy levels.

I. INTRODUCTION

Energy harvesting of heat dissipated from electronic circuits and other heat sources is one of the most important energy issues.[1] The realization of such type of energy harvesting typically relies on the search of thermoelectric (TE) materials with high figure of merits (ZT).[2] Impressive ZT values for quantum-dot superlattices (QDSL) systems have been demonstrated experimentally.[3] The enhancement of ZT mainly arises from the reduction of phonon thermal conductivity in QDSL, which is due to the increased rate of phonon scattering from the interface of quantum dots (QDs).[1,2] If the ZT value can reach 3, the solid state cooler will have the potential to replace conventional compressor-based air conditioners owing to its long life time, low noise and low air pollution. Besides the search of TE devices with large ZT value, the optimizing of nonlinear thermoelectric behavior under high temperature bias is crucial for the design of the next-generation energy harvesting engine (EHE).[1,2]

Recently, a great deal of efforts was devoted to the studies of the nonlinear response of thermoelectric devices under high temperature bias. The nonlinear phonon flow of nanostructures with respect to large temperature bias were investigated experimentally[4] and theoretically.[5-8] The phonon thermal rectification behavior of silicon nanowire (which has a very low efficiency) was reported experimentally.[4] More recently, the highly efficient electron thermal diode was reported in a superconductor junction system.[9] However, such a thermal rectification behavior only exists at very low temperatures. Unlike heat rectifiers which are used to

control the direction of heat flow [4-9], the design of an EHE driven by a large temperature bias needs to optimize the efficiency in the energy transfer from the waste heat[1,2]. Although the energy harvesting of coupled double QDs with size near $1\mu m$ was reported experimentally and theoretically,[10-12] the large-size QDs typically have charging energy (U) much larger than energy separation (ΔE). To design EHE operated at room temperature, we need to consider QDs with nanoscale size, satisfying the condition of $\Delta E/U \gg 1$ to emphasize the focus of our current study.

So far, experimental studies of EHE made of nanoscale semiconductor QD molecules (QDMs) or molecules have not been reported, mainly due to technical difficulties[13] (for example, an isolated single nanowire or a molecular chain connected with electrodes) and the lack of good theoretical designs. Therefore, it is desirable to have theoretical studies which can provide useful guidelines for the advancement of nanoscale TE technology. The most challenging issue for theoretical studies arises from the strong electron Coulomb interactions in semiconductor QDMs or realistic molecules. Many techniques such as rate equation, master equation and numerical renormalization group method were used to examine the TE properties of QD junction system.[14-24]. Most theoretical studies of TE properties have focused on the linear response regime.[14-20] The TE properties of molecular junction system beyond linear response were theoretically reported in references[21-24]. However, the many-body effects arising from orbital-filling on the nonlinear TE properties of QDMs or molecules are still not clear. Such effects are crucial when the energy levels of QDM are below the Fermi energy of electrodes.[20] Under high tem-

perature bias, the thermal-bias induced electrical current will cause a voltage drop due to the load resistance, which in turn will also modify the current. Thus, the theoretical design of such an EHE must solve the thermal-induced electrical voltage in a self-consistent way. In this article, we describe such a self-consistent approach to study the nonlinear behavior of EHE made of double QDs and serially coupled triple QDs (SCTQDs). The comparison of the results for DQD and SCTQD allows one to see the trend of increasing the length of chain of QD molecules. Our studies are based on numerical method as described in [25], which can suitably address the full many-body effect in the Coulomb blockade regime for coupled multiple QDs. Due to the many-body effect, the maximum efficiency of EHE made of the SCTQDs occurs only in the orbital depletion regime. Meanwhile, we also clarify how the efficiency of EHE is influenced by the physical parameters of SCTQDs. In addition, we investigate an engine with direction-dependent electrical output driven by a temperature-bias for application as a novel TE devices.

II. THEORETICAL METHOD

The insets of Figures 1 and 2 show the QD molecule (QDM) connected to two metallic electrodes, one is in thermal contact with the heat source at temperature T_H (hot side) and the other with the heat sink kept at temperature T_C (cold side). The heat flows from the hot side through the QDM into the cold side. To reveal the electron and heat currents driven by the temperature bias, we consider the following Hamiltonian $H = H_0 + H_{QD}$ for a QDM junction system:

$$H_0 = \sum_{k,\sigma} \epsilon_k a_{k,\sigma}^\dagger a_{k,\sigma} + \sum_{k,\sigma} \epsilon_k b_{k,\sigma}^\dagger b_{k,\sigma} \quad (1)$$

$$+ \sum_{k,\sigma} V_{k,L} d_{L,\sigma}^\dagger a_{k,\sigma} + \sum_{k,\sigma} V_{k,R} d_{R,\sigma}^\dagger b_{k,\sigma} + c.c$$

where the first two terms describe the free electron gas of left and right electrodes (hot and cold sides). $a_{k,\sigma}^\dagger$ ($b_{k,\sigma}^\dagger$) creates an electron of momentum k and spin σ with energy ϵ_k in the left (right) electrode. $V_{k,\ell}$ ($\ell = L, R$) describes the coupling between the electrodes and the left (right) QD. $d_{\ell,\sigma}^\dagger$ ($d_{\ell,\sigma}$) creates (destroys) an electron in the ℓ -th dot.

$$H_{QD} = \sum_{\ell,\sigma} E_\ell n_{\ell,\sigma} + \sum_{\ell} U_\ell n_{\ell,\sigma} n_{\ell,\bar{\sigma}} \quad (2)$$

$$+ \frac{1}{2} \sum_{\ell,j,\sigma,\sigma'} U_{\ell,j} n_{\ell,\sigma} n_{j,\sigma'} + \sum_{\ell,j,\sigma} t_{\ell,j} d_{\ell,\sigma}^\dagger d_{j,\sigma}$$

where E_ℓ is the spin-independent QD energy level, and $n_{\ell,\sigma} = d_{\ell,\sigma}^\dagger d_{\ell,\sigma}$. Notations U_ℓ and $U_{\ell,j}$ describe the intradot and interdot Coulomb interactions, respectively.

$t_{\ell,j}$ describes the electron interdot hopping. Noting that the interdot Coulomb interactions as well as intradot Coulomb interactions play a significant role on the electron transport in semiconductor QD arrays or molecular chains.[15, 16] Because we are interested in the case that the thermal energy is much smaller than intradot Coulomb interactions, we consider QDs with only one energy level per dot.

Using the Keldysh-Green's function technique,[26,27] the electron and heat currents from reservoir α to the QDM junction are calculated according to the Meir-Wingreen formula given by

$$J_\alpha = \frac{ie}{\hbar} \sum_{j\sigma} \int \frac{d\epsilon}{2\pi} \Gamma_j^\alpha(\epsilon) [G_{j\sigma}^<(\epsilon) + f_\alpha(\epsilon)(G_{j\sigma}^r(\epsilon) - G_{j\sigma}^a(\epsilon))] \quad (3)$$

$$Q_\alpha = \frac{i}{\hbar} \sum_{j\sigma} \int \frac{d\epsilon}{2\pi} (\epsilon - \mu_\alpha) \Gamma_j^\alpha(\epsilon) [G_{j\sigma}^<(\epsilon) + f_\alpha(\epsilon)(G_{j\sigma}^r(\epsilon) - G_{j\sigma}^a(\epsilon))] \quad (4)$$

Here $\Gamma_j^\alpha(\epsilon) = \sum_k \delta(\epsilon - \epsilon_k) |V_{k,\alpha}|^2$ is the tunneling rate between the left (right) reservoir and the left (right) QD of QDM. For the simplicity, we consider the wide band limit of electrodes to ignore energy-dependent tunneling rates $\Gamma_{L(R)}^{L(R)}(\epsilon) = \Gamma_{L(R)}$. $f_\alpha(\epsilon) = 1/\{\exp[(\epsilon - \mu_\alpha)/k_B T_\alpha] + 1\}$ denotes the Fermi distribution function for the α -th electrode, where μ_α and T_α are the chemical potential and the temperature of the α electrode. $\mu_L - \mu_R = -e\Delta V$ and $T_L - T_R = \Delta T$. e , \hbar , and k_B denote the absolute value of electron charge, the Planck's constant, and the Boltzmann constant, respectively. $G_{j\sigma}^<(\epsilon)$, $G_{j\sigma}^r(\epsilon)$, and $G_{j\sigma}^a(\epsilon)$ are the frequency domain representations of the one-particle lesser, retarded, and advanced Green's functions $G_{j\sigma}^<(t, t') = i\langle d_{j,\sigma}^\dagger(t') d_{j,\sigma}(t) \rangle$, $G_{j\sigma}^r(t, t') = -i\theta(t - t') \langle \{d_{j,\sigma}(t), d_{j,\sigma}^\dagger(t')\} \rangle$, and $G_{j\sigma}^a(t, t') = i\theta(t' - t) \langle \{d_{j,\sigma}(t), d_{j,\sigma}^\dagger(t')\} \rangle$, respectively. These one-particle Green's functions are related recursively to other Green's functions and correlation functions via a hierarchy of equations of motion (EOM).[28] We truncate the equation of motion by integrating out the leads degrees of freedom using the Markov approximation, so the Kondo physics [29] is ignored. By doing so we can focus on solving the Green's function within the triple quantum dots system with the effects due to coupling to leads approximated by a constant self-energy term, and the hierarchy of EOM self-terminates at the level of $2N$ -particle Green's functions for the N -QD system (with $2N$ levels, including spin). We have considered the Pauli exclusion principle and charge conservation. For SCTQDs with one energy level in each QD, there are 6 energy levels (including spin). In the steady state, the number of Green's functions (involving up to six particles) described by $\langle d_{i_1}^\dagger \dots d_{i_{n-1}}^\dagger d_{j_1} \dots d_{j_n}(t) d_{j'}^\dagger(t') \rangle$ ($n = 1, \dots, 6$) is given by $\sum_{n=1}^6 \binom{6}{n-1} \times \binom{6}{n} \times 6 = 4752$. Using charge conservation ($U(1)$ symmetry), the number of correlation

functions $\langle d_{i_1}^\dagger \dots d_{i_n}^\dagger d_{j_1} \dots d_{j_n} \rangle$ needed to be solved can be reduced to $\sum_{n=1}^6 \binom{6}{n}^2 = 923$. The self-consistent solution to these equations are solved numerically according to procedures described in refs. [20] and [30]. The algorithms employed are numerically stable, and for equilibrium systems the code gives exactly the same results as those obtained by exact diagonalization. In this paper, we compare results obtained by the full calculation (method A) and a simplified calculation (method B) to reveal the many-body effect on the EHE efficiency. In method A, we calculate the electron and heat currents of Eqs. (3) and (4) by considering all correlation functions resulting from electron Coulomb interactions. Both methods are valid only in the Coulomb blockade regime, not the Kondo regime. In the case of DQD the method A gets exactly the same results for tunneling current as reported in Ref. [28].

With method A it is difficult to illustrate the behaviors of electron and heat currents due to the lack of simple analytic expressions. In method B, we neglect all correlations functions except the two-electron correlation function for electrons on the same site, whereas we still consider all many-body Green functions (up to six electrons). This simplified method allows us to obtain the expressions of electron and heat currents in terms of an analytic function, $\mathcal{T}_{LR}(\epsilon)$ called transmission coefficient. Their expressions are

$$J = \frac{e}{h} \int d\epsilon \mathcal{T}_{LR}(\epsilon) [f_L(\epsilon) - f_R(\epsilon)], \quad (5)$$

and

$$Q_{L/R} = \pm \frac{1}{h} \int d\epsilon (\epsilon - \mu_{L(R)}) \mathcal{T}_{LR}(\epsilon) [f_L(\epsilon) - f_R(\epsilon)]. \quad (6)$$

Because there are four possible states for each QD level (empty, one spin-up electron, one spin-down electron, and two electrons), $\mathcal{T}_{LR}(\epsilon)$ contains $4^3 = 64$ configurations for the SCTQD. The expression of $\mathcal{T}_{LR}(\epsilon)$ can be found in Ref. 31, in which only one-particle occupation numbers and two-particle on-site correlation functions used in the Green's functions are considered. Method B requires much less computation effort than the full calculation and can take advantage of the analytic expression for $\mathcal{T}_{LR}(\epsilon)$. Therefore, method B is very useful in clarifying the physical mechanisms responsible for the results obtained by the full calculation (method A).

To design an EHE driven by a high temperature-bias ΔT , the thermal induced voltage ($-eV_{th} = \mu_L - \mu_R$) across the external load with conductance $G_{ext} = 1/R_{ext}$ needs to be calculated. To obtain eV_{th} , we have to solve self-consistently all correlation functions appearing in the electron current subject to the condition $G_{ext}V_{th} = J$, where $J = (J_L + J_R)/2$ is the net electron current. The heat current satisfies the condition $Q_L + Q_R = J \times V_{th}$, which denotes the work done by the EHE per unit time. The efficiency of EHE is thus given by

$$\eta = |J * V_{th}|/Q_L. \quad (7)$$

In the following discussions, we will illustrate the nonlinear electron transport of EHE mostly based on the full calculation and some based on the simplified calculation (method B) for comparison.

III. RESULTS AND DISCUSSION

An EHE made of a single QD with one energy level was theoretically studied in Refs. 32 and 33. To reveal the electron coherent tunneling effect on the efficiency of EHE, the case of DQD under a fixed temperature difference ΔT and electrical voltage ΔV was studied in Ref. 34. They then evaluate the EHE efficiency according to $\eta = |J * V|/Q_L$. In the realistic operation of an EHE, there is a fixed external load with resistance R_{ext} . Since the voltage drop across the load must satisfy the relation $\Delta V = JR_{ext}$, it can be argued that in Refs. 32-34 an external resistance $R_{ext} = \Delta V/J$ was assumed. However, when the EHE efficiency η is examined as a function of some external parameter (such as the gate voltage), keeping a fixed ΔV becomes unphysical, since it implies a continuous change of the load resistance as the external parameter varies. A more physical way to study the dependence of η is to calculate the thermal-induced bias (V_{th}) (arising from the Seebeck effect) self-consistently for a fixed load.

Here, we consider a fixed load with conductance $G_{ext} = 1/R_{ext} = 0.2G_0$, where $G_0 = 2e_0^2/h$. Based on the full calculation and Eq. (7), we obtain the electron current (J), thermal-induced bias (V_{th}) and efficiency (η) of DQD as a function of QD energy level tuned by gate-voltage ($E_L = E_R = E_F + 30\Gamma_0 - eV_g$) for various T_C values with $\Delta T = 1\Gamma_0$. The results are shown in Fig. 1. We found bipolar oscillatory behaviors for J and V_{th} with respect to QD energy level, similar to the behavior of Seebeck coefficient (S). Such an oscillatory behavior was experimentally reported in a single metallic QD case.[35] There are four main structures in the J , V_{th} and η curves, which correspond to processes of electrons tunneling through the DQD in the one-, two-, three-, and four-electron states, respectively. The maximum η occurs either in the orbital-depletion regime (with DQD in the one-electron state) or in the full orbital-filling regime (with DQD occupied by four electrons). The suppression of η due to increasing T_C is also illustrated in this figure.

To gain deeper insight of the results shown in Fig. 1(c), we consider the expression of η_{ZT} derived by the classical approach given in Refs. 1 and 2.

$$\eta_{ZT} = \left(\frac{\Delta T}{T_C + \Delta T} \right) \frac{m}{m + (1 + m)^2 / (ZT_H) + \bar{T}/T_H}, \quad (8)$$

where $m = G_e/G_{ext}$, and $Z = \frac{S^2 G_e}{\kappa}$. G_e , $S = V_{th}/\Delta T$, and $\kappa = \kappa_e + \kappa_{ph}$ are the electrical conductance, Seebeck coefficient, and thermal conductance of the EHE. κ_e and κ_{ph} are the electron and phonon thermal conductance, respectively. $\bar{T} = (T_H + T_C)/2$. When T_H approaches T_C ,

ZT_H becomes the dimensionless "Figure of merit" in the linear response regime. Eq. (8) reveals that the EHE becomes a Carnot engine with $\eta_C = \Delta T / (T_C + \Delta T)$ as ZT approaches infinity and $m \gg 1$. Obviously, the suppression of maximum η with increasing T_C can be illustrated by η_C . From Eq. (8) we can deduce that high-efficiency TE devices require large ΔT and ZT values, which in general coincide with the condition of small thermal conductivity.

Composite materials with high density of QDs embedded in a low κ_{ph} material can in general lower the thermal conductivity. For practical application, one should consider the case of N-QDs between two metallic electrodes. However, due to the very complicate many-body effect resulting from N-QDs, here we only focus on the DQD and SCTQD systems and compare the results to see the trend.

It is nontrivial to analyze the electron currents in the nonlinear response regime with respect to a large temperature bias as many-body effects can not be avoided in SCTQDs.[36-39] The analysis of electron current spectra becomes very intriguing. To clarify how the resonant channels of SCTQD resulting from electron Coulomb interactions influence the electron transport, we compare the calculated electron current for a fixed electrical voltage with $e\Delta V = 1\Gamma_0$ and $\Delta T = 0$ to that for a short-circuit case ($\Delta V = 0$ or $R_{ext} = 0$) with $k_B\Delta T = 1\Gamma_0$, and the results are shown in Fig. 2. In this case, it is relatively easy to analyze the electron current spectra of SCTQDs. Figure 2(a) shows the total occupation number ($N_t = \sum_{\sigma} (\langle n_{L\sigma} \rangle + \langle n_{C\sigma} \rangle + \langle n_{R\sigma} \rangle)$) of SCTQD without thermal bias ($k_B\Delta T = 0$) as a function of the applied gate voltage V_g for three different temperatures ($k_B T_C = 1, 3, 5\Gamma_0$). The electrical bias is set at $e\Delta V = 1\Gamma_0$. The staircase behavior of N_t is due to the charging effect arising from electron intradot and interdot Coulomb interactions. The average occupancies in the center dot ($\langle n_{C\sigma} \rangle = N_{C,\sigma}$) and outer dots ($\langle n_{L\sigma} \rangle (N_{L,\sigma}) = \langle n_{R\sigma} \rangle (N_{R,\sigma})$) are also plotted in Fig. 2(a) as dash-double-dots and dash-dotted curves, respectively. Because of symmetry, the average occupancies in two outer dots remain the same as V_g varies, which leads to a jump of 2 for N_t for the first two steps.

The corresponding tunneling currents $J_{\Delta V}$ are plotted in Fig. 2(b). The negative sign of $J_{\Delta V}$ labeled by ϵ_1 and ϵ_2 indicates that the electron current is flowing from the right electrode to the left electrode. The tunneling currents are appreciable only in the regions where N_t jumps a step, but become blocked when N_t is flat as a function of eV_g . J_{max} is suppressed with increasing temperature (T_C). Although many efforts have been devoted to studies of electron transport through SCTQDs under an applied bias [36-39], not many literatures studied the electron current through SCTQD under high temperature bias.

Fig. 2(c) shows the electron current driven by a temperature bias for various values of $k_B T_C$ with $\Delta V = 0$. We note that $J_{\Delta V}$ and $J_{\Delta T}$ are vanishingly small when

N_t varies from four to five. This is due to the lack of resonant channel in SCTQD, which leads to $E_L + U_0 + U_{LC} = E_R + U_0 + U_{CR} \neq E_C + 2U_{LC} + 2U_{CR}$ and therefore the electron transport is blocked. Such an effect also exists for the change of N_t from five electrons to six electrons (not shown here).

In the practical operation of EHE, a temperature bias ΔT should induce a thermal voltage V_{th} ($-eV_{th} = \mu_L - \mu_R$) which depends not only on the load conductance G_{ext} but also on the correlation functions resulting from electron Coulomb interactions. Such behavior is illustrated in Fig. 3, which shows the electron current (J), thermal-bias induced voltage (V_{th}) and η driven by a temperature bias at $k_B\Delta T = 1\Gamma_0$ for various values of $k_B T_C$. Comparing with Fig. 2(c), we see that the behavior of electron current (J) is qualitatively similar to the case with $R_{ext} = 0$. However, the magnitude is reduced by about 30% when $G_{ext} = 0.2G_0$ due to the counter balancing effect through the thermal-bias induced voltage V_{th} . Both J and $-eV_{th}$ shown in Fig. 3 display a bipolar oscillatory behavior, similar to that shown in Fig. 1(a). In the orbital depletion regime, the behaviors of SCTQD are very similar to those of DQD, whereas deviation occurs (with the efficiency (η) lowered by about 30% compared with DQD) when QD energy levels are below E_F . η becomes even lower at higher V_g due to the lack of resonant channels in SCTQD (caused by the blockade of electron transport from interdot Coulomb interactions). In the absence of U_I , η can be higher even for higher V_g . We see that the highest efficiency of EHE occurs near the transition where N_t goes from 0 to 1 (with $eV_g \approx 25\Gamma_0$), which is in the orbital-depletion regime.

To reveal the importance of electron correlation arising from many body effect, the physical quantities of Fig. 3 are recalculated by method B. The resulting curves are shown in Fig. 4, which have one-to-one correspondence to those of Fig. 3. For the low-filling situation (with $eV_g < 30\Gamma_0$), the results agree very well with the full-calculation results shown in Fig. 3. On the other hand, there are appreciable differences between the two results as N_t exceeds 1 (with $eV_g > 30\Gamma_0$), although their behaviors are qualitatively the same for eV_g up to $100\Gamma_0$. This implies that a simplified model without considering interdot correlation functions is sufficient to model the main characteristics of the EHE made of SCTQDs in the low-filling regime ($N_t \leq 1$).

So far, we have fixed $G_{ext} = 0.2G_0$ and neglected the phonon heat flow ($Q_{ph} = 0$). In the inset of Fig. 4, we show results for $\eta = |J \times V_{th}| / (Q_L + Q_{ph})$ versus V_g for four different values of G_{ext} at $k_B T_C = 1\Gamma_0$ with $k_B\Delta T = 1\Gamma_0$ and $t_C = 1\Gamma_0$, where we have included the effect of phonon heat flow given by a simple model $Q_{ph} = \kappa_{ph,0} F_s \Delta T$. (F_s is the correction factor describing the phonon scattering resulting from the surface of nanowires and the QDs) Here, $\kappa_{ph,0} = \frac{\pi^2 k_B^2 T}{3h}$ is the universal phonon thermal conductance arising from acoustic phonon confinement in a nanowire. It is generally accepted that the linear term of phonon thermal con-

ductivity $\kappa_{ph,0}$ can well illustrate the behavior of silicon nanowire even at room temperature.[40] In a nanowire filled with QDs considered in our paper, photon scattering is dominated by the defect scattering (due to structure difference between QDs and nanowire), which implies that the phonon mean-free path, ℓ is not sensitive to the temperature variation. The linear dependence in temperature comes from the specific heat C , which is proportional the phonon density of states in one dimension, thus linearly proportional to temperature. According to the relation $\kappa = Cv\ell$, we obtain a linear temperature dependence for κ , since the sound velocity (v) is also not very sensitive to temperature. Furthermore, the physics for the reduction of η in the presence of Q_{ph} will remain qualitatively similar even if there is small nonlinear effect in κ_{ph} in the temperature range considered. Recently, phonon thermal conductivity in the Kondo regime (extremely low temperature regime) has been investigated in Ref. 42. The maximum efficiency is obtained at $G_{ext} = 0.05G_0$. Meanwhile, the maximum η for $G_{ext} = 0.2G_0$ (blue line) is around 0.08 including the effect of Q_{ph} , which is about one half of the value obtained with $Q_{ph} = 0$ as shown by the black solid line in Fig. 4(c). According to Eq. (6), the optimized η_{ZT} occurs at $G_{ext}^o = G_e/\sqrt{1+Z\bar{T}}$. Thus, η_{max} will occur at vanishingly small G_{ext} if $Z\bar{T}$ becomes very large. When $Z\bar{T} = 2$, $G_{ext}^o = G_e/\sqrt{3} \approx 0.047G_0$ for $G_e = 0.08G_0$. This is consistent with the results shown in the inset of Fig. 4, where η_{max} occurs near $G_{ext}^o = 0.05G_0$.

To illustrate the effect of thermal-bias induced voltage, we also calculate the electron current and heat current of SCTQD as functions of gate voltage V_g for the case of a fixed electrical voltage with $e\Delta V = 1\Gamma_0$ based on method B. Note that this situation corresponds to a load conductance G_{ext} which varies with V_g with the relation $G_{ext} = J/\Delta V$. Fig. 5(a) shows the bipolar behavior of the electron current, which is qualitatively similar to the results shown in Fig. 4(a) except that the magnitude of J is much smaller here. In Fig 5(b) we show the heat currents obtained for fixed $e\Delta V = 1\Gamma_0$ (solid curves) as well as the results for a fixed load with $G_{ext} = 0.2G_0$ (dashed curves). It is noted that Q_L becomes negative for $k_B T_C = 3\Gamma_0$ (red solid curve) and $5\Gamma_0$ (blue solid curve) for eV_g around $28\Gamma_0$. Such negative values are caused by the negative load conductance $G_{ext} = J/\Delta V$ implicitly adopted, where J becomes negative for $\Delta V = 1\Gamma_0$. Such a situation does not correspond to a realistic operation of EHE. Once we consider a fixed load and find the self-consistent solution to V_{th} , the heat currents are always positive (as shown by dashed curves). Because of this issue, in Refs. 32-34, the η value of EHE can only be evaluated for the area of Q_L larger than zero. From the comparison of results in Fig. 5(b), we see that it is important to include V_{th} in a self-consistent way in the optimization of η for EHE. The inset of Fig. 5 shows the efficiency of EHE as functions of G_{ext} for different $k_B\Delta T$ values at $eV_g = 28\Gamma_0$ and $k_B T_C = 1\Gamma_0$ in the absence of Q_{ph} . The maximum η occurs at $G_{ext} = 0.01G_0$, which

is smaller than that for the case with Q_{ph} . This also indicates that the ZT value of SCTQD is highly enhanced in the absence of κ_{ph} . For a fixed G_{ext} , η is enhanced with increasing ΔT in the orbital depletion region.

So far, we have focused on a fixed electron hopping strength $t_C = 1\Gamma_0$. It is also interesting to examine how η is influenced when t_C increases. We plot J , Q_L and η as functions of t_C for $E_0 = E_F + 2\Gamma_0$ and $eV_g = 0$ in Fig. 6 based on method B. To illustrate the results of Fig. 6, the approximated expression of $\mathcal{T}_{LR}^1(\epsilon)$ is given below:

$$\mathcal{T}_{LR}^1(\epsilon) = \frac{4\Gamma_L\Gamma_R P_1 t_{LC}^2 t_{CR}^2}{|\mu_1\mu_2\mu_3 - t_{CR}^2\mu_1 - t_{LC}^2\mu_3|^2}, \quad (9)$$

where $\mu_1 = \epsilon - E_L + i\Gamma_L$, $\mu_2 = \epsilon - E_C$ and $\mu_3 = \epsilon - E_R + i\Gamma_R$. $P_1 = (1 - N_{L,\bar{\sigma}})(1 - N_{C,\bar{\sigma}} - N_{C,\sigma} + c_C)(1 - N_{R,\bar{\sigma}} - N_{R,\sigma} + c_R)$ denotes the probability weight of electron transport through SCTQD in an empty state, which is determined by the one particle occupation number ($N_{\ell,\bar{\sigma}}$) and on-site two particle correlation functions (c_ℓ) resulting from electron Coulomb interactions. Only, the first of 64 configurations for SCTQD is included in Eq. (9), because the QD energy levels are above E_F . P_1 equals to one in the absence of electron Coulomb interactions.[30] We derive the expression of tunneling current in the small tunneling rate limit ($\Gamma/k_B\bar{T} \ll 1$) under the assumption $\Delta T/\bar{T} \ll 1$ and obtain

$$J = \frac{2e}{h} \frac{\pi\Gamma P_1}{k_B\bar{T}^2} \frac{4t_{LC}^2 t_{CR}^2 (E_0 - E_F)}{(t_{LC}^2 + t_{CR}^2 + \Gamma^2)^2} \frac{\Delta T}{\cosh^2 \frac{E_0 - E_F}{2k_B\bar{T}}}. \quad (10)$$

From Eq. (10), we see that the maximum J occurs when $t_{LC} = t_{CR} = t_C$. Thus, non-uniform electron hopping strength tends to reduce J . Meanwhile, the maximum J and η occur at $t_C = \Gamma_0/\sqrt{2}$, which well explains the results of Fig. 6(a). In addition, the suppression of J with increasing T_C can also be described by Eq. (10). Note that tunneling current arising from V_{th} has been neglected in Eq. (10). From the results of Fig. 6, we see that J and Q_L are not a monotonic function of t_C . Because $t_{LR} = 0$ in this calculation, we do not observe the interesting quantum interference effect (QIE). In Ref. [20], how QIE influences electrical conductance, Seebeck coefficient and electron thermal conductance was discussed in the case of triangular TQD.

To further examine the behavior of the EHE efficiency, we plot in Fig. 7 J , Q_L and η as functions of V_g for various values of $k_B\Delta T$ with T_C fixed at $1\Gamma_0$ and $G_{ext} = 0.05G_0$. We see that the peak values of J , Q_L and η all increase with ΔT . It is worth noting that Q_L is positive in the entire parameter space (unlike the electron current which shows bipolar oscillatory behavior with respect to QD energy level). The results of Fig. 7 indicate that a high efficiency engine with large electrical outputs requires a high temperature bias, which exists only in a system with high thermal resistivity (phonon glass). Serially coupled QDs can enhance the phonon scattering and thus reduce thermal conductivity. Therefore, a long chain of

QD molecules is desirable for implementing EHE with high efficiency. As for the optimization length of QD molecules, this problem is beyond the scope of present article. There are two reasons: (a) the model of phonon heat flow is too simple to fully catch the realistic phonon heat flow magnitude, and (b) the calculation of QD number beyond three requires the high cost computing time. For most conventional TE devices, there exist a trade-off between high efficiency and large output power. Based on the results presented in Figs. (3)-(6), it is concluded that a high-efficiency EHE should operate in the low-filling regime. Because the effect of Q_{ph} is important (as eluded in the inset of Fig. 4), we also calculate the EHE efficiency including the Q_{ph} effect. The results for $k_B\Delta T = 3\Gamma_0$ are shown as triangles, which is to be compared with the dotted line of Fig. 7(c). Obviously, η_{max} is suppressed when Q_{ph} is included. However, we note that the maximum η can still reach a maximum close to 0.2 in the presence of Q_{ph} . This is considered high efficiency when compared with conventional heat engines[1,2].

When there is size/shape variation in serially coupled QDs, three important physical quantities including the electron Coulomb interactions, tunneling rates and QD energy levels will be changed. In the depletion regime with the best engine efficiency, the energy level fluctuation (ELF) of QDs will cause a significant effect on the ZT values. Therefore, it is desirable to examine the ELF effect on the electron current (or EHE efficiency) of SCTQD. In general, we found that the EHE efficiency is suppressed by ELF in SCTQDs mainly due to the reduced electron current. However, we found that a staircase alignment of QD energy levels can be used to design an engine with direction-dependent electrical output. In Fig. 8, the electron current (J) and thermal voltage (V_{th}) are calculated for an SCTQD with staircase-like alignment of energy levels: $E_L = E_R + 2\Delta$, $E_C = E_R + \Delta$ and $E_R = E_F + 10\Gamma_0$, where Δ is the QD energy level difference. In Figs (1)-(7), we have neglected the voltage drop across the dots due to V_{th} . To examine such an effect we show in Fig. 8 the influence due to the change of outer QD energy levels arising from V_{th} , which follows the relation $\epsilon_{L(R)} = E_{L(R)} \mp D_\eta eV_{th}$. It's worth noting that the tunable factor D_η is mainly determined by the QD separation. Here, we adopt $D_\eta = 0.3$. For $\Delta T > 0$ ($\Delta T < 0$), T_H is on the left (right) electrode (See insets of Fig. 8(a)). The forward (backward) currents ($J_{F(B)}$) are positive (negative), while V_{th} has opposite sign with respect to J . Both forward and backward electron currents have a nonlinear dependence on ΔT . With increasing Δ , the electron currents (or electrical powers) are suppressed in the wide temperature bias regime. For $\Delta = 0$ (solid black curve), the electron current shows no directionality, while for $\Delta = 2\Gamma_0$ the direction-dependent electron current becomes apparent. This directionality of electron current can be qualitatively explained as follows. When $\Delta T > 0$, ϵ_L and ϵ_R become aligned with E_C as $-eV_{th}$ changes to around $-2\Gamma_0$, while for $\Delta T < 0$, ϵ_L and ϵ_R are tuned further away from E_C . Therefore, QD energy level shift

due to the thermal-induced voltage can play a remarkable role for the current rectification effect in SCTQD with staircase-like energy levels. The energy level shift of QDs arising from thermal voltage was experimentally observed in the DQD realized by lithographic technique.[43] The experiment of Ref. 43 is limited to the low temperature regime with a small temperature bias, since the QDs considered are large and the charging energies are much larger than the energy level separation. If V_{th} is turned off, we can no longer observe direction-dependent tunneling current under temperature bias even though SCTQD has site-dependent QD energy levels.

Let's define the electron current rectification efficiency as $\eta_R = (J_F - |J_B|)/|J_F + |J_B||$, which is irrelevant to heat flows. The calculated η_R as a function of temperature bias under various conditions is shown in Fig. 9. Figure 9(a) shows η_R for various values of Δ with $t_C = 3\Gamma_0$. We see that the highest rectification occurs when $\Delta = 2\Gamma_0$ with η_R approaching 0.2 at the high ΔT limit. The rectification efficiency actually becomes poorer if Δ is too large. Unlike the case with $\Delta = 2\Gamma_0$, η_R decreases with increasing ΔT for $\Delta = 4$ and $6\Gamma_0$. To reveal the electron correlation effects, we also calculate η_R with method B and plot the corresponding curves with triangle marks in Fig. 9(a). It is found that the rectification efficiency is overestimated in this simplified model. When a temperature bias increases significantly, the total occupation (N_t) increases. Therefore, electron-correlation effect becomes strong. In particular, the interdot two-electron correlation functions can no longer be ignored. This explains why the numerical results of method B (with less correlation functions) becomes overestimated. Figure 9(b) shows η_R for $\Delta = 2\Gamma_0$ for different electron hopping strengths ($t_C = 0.5, 1$, and $2\Gamma_0$). η_R is found to be largest for $t_C = 2\Gamma_0$ (dotted line), which is also larger than that for $t_C = 3\Gamma_0$ as shown in Fig. 9(a). Thus, the electron current rectification efficiency is not a monotonic function of t_C . In Fig. 9(c), we consider the effect of varying the temperature of the cold side, T_C . The results indicate that the maximum η_R reduces with increasing T_C .

Nonlinear thermoelectric effects of nanostructures for developing new applications have been reviewed in a recent article.[44] For phonon rectifiers, it is very difficult to realize "phonontronics" due to large leakage of phonon flow arising from acoustic phonons, which are difficult to confine.[4-6,12] The heat rectification phenomena of electrons can only exist at low temperatures, where phonon flows can be suppressed.[7-9,12] On the other hand, the electron current rectification shown in Fig. 9 will be unaffected by the phonon flow. Therefore an EHE made of serially coupled QDs with direction-dependent electrical current may prove useful in the advancement of nonlinear thermoelectric devices.[45]

IV. SUMMARY

The electron/heat transport in nanoscale semiconductor QDM driven by a finite temperature bias is theoretically studied for the application of EHE, which converts thermal energy into electrical power. Our studies illustrate that the efficiency of the EHE made of QDM must be evaluated by Eqs. (3) and (4) under the constraint $G_{ext} V_{th} = J$, in which V_{th} induced by ΔT should be calculated self-consistently, otherwise the J and Q will show nonphysical features. We have demonstrated that an EHE made of a DQD has high efficiency either in the charge-depletion or full-filling regime, whereas an EHE made of SCTQD prefers the charge-depletion regime due to the lack of resonant channels in the full-filling regime. We found that the EHE performance is degraded by the energy-level fluctuation (ELF) in QDs, which may arise from QD size variation or energy level shift caused by thermal voltage V_{th} . η_{max} of EHE is seriously suppressed in the presence of phonon thermal conductance. QDMs have promising potential for realizing high-efficiency EHEs due to their low phonon thermal conductance. The direction-dependent electron current is illustrated by an SCTQD with staircase-like energy levels. The thermal voltage yielded by temperature bias

plays a remarkable role in the design of an engine with bidirectional current driven by a temperature bias. The results of Fig. 9(a) clearly reveal that interdot electron correlation functions arising from electron Coulomb interactions (considered in method A) play a significant role in the high temperature bias regime. The condition of $\Delta E/U \gg 1$ for each QD can be satisfied for small molecules such as benzene. (See Refs. [15] and [16]). Therefore, our study is applicable for studying finite benzene chain.

Acknowledgments

This work was supported by the National Science Council of the Republic of China under Contract Nos. MOST 103-2112-M-008-009-MY3 and MOST 104-2112-M-001-009-MY2.

[†]Present address: Department of Physics, Zhejiang University, Hangzhou 310027, China

^{††}E-mail address: mtkuo@ee.ncu.edu.tw

*E-mail address: yiachang@gate.sinica.edu.tw

-
- ¹ A. J. Minnich, M. S. Dresselhaus, Z. F. Ren, and G. Chen, *Energy Environ. Sci.* **2**, 466 (2009).
- ² M. Zebarjadi, K. Esfarjania, M.S. Dresselhaus, Z.F. Ren and G. Chen, *Energy Environ Sci* **5**, 5147 (2012).
- ³ T. C. Harman, P. J. Taylor, M. P. Walsh, B. E. LaForge, *Science* **297**, 2229 (2002).
- ⁴ C. W. Chang, D. Okawa, A. Majumdar, and Zettl A, *Science* **314**, 1121 (2006).
- ⁵ B. W. Li, L. Wang and G. Casati, *Phys. Rev. Lett.*, **93**, 184301 (2004).
- ⁶ B. Hu, L. Yang, and Y. Zhang, *Phys. Rev. Lett.* **97**, 124302 (2006).
- ⁷ D. M. T. Kuo and Y. C. Chang, *Phys. Rev. B* **81**, 205321 (2010).
- ⁸ Y. C. Tseng, D. M. T. Kuo, Y. C. Chang and Y. T. Lin, *Appl. Phys. Lett.* **103**, 053108 (2013).
- ⁹ M.J. Martinez, A. Fornieri and F. Giazotto, *Nature Nanotechnology*, **10**, 303 (2015).
- ¹⁰ F. Hartmann, P. Pfeffer, S. Hoffling, M. Kamp, and L. Worschech, *Phys. Rev. Lett.* **114**, 146805 (2015).
- ¹¹ B. Roche, P. Roulleau, T. Jullien, Y. Jompol, I. Farrer, DA Ritchie, and DC Glattli, *Nature communications*, **6**, 6738 (2015).
- ¹² H. Thierschmann, R. Sanchez, B. Sothmann, F. Arnold, C. Heyn, W. Hansen, H. Buhmann, and LW Molenkamp, *Nature nanotechnology*, **10**, 854 (2015).
- ¹³ T. K. Hsiao, H. K. Chang, S. C. Liou, M.W. Chu, S. C. Lee, and C. W. Chang, *Nature Nanotechnology* **8**, 534 (2013).
- ¹⁴ X. Zianni, *Phys. Rev. B* **75**, 045344 (2007).
- ¹⁵ J. P. Bergfield and C. A. Stafford, *Nano Letters* **9**, 3072 (2009).
- ¹⁶ J. P. Bergfield, M. A. Solis, and C. A. Stafford, *ACS Nano* **4**, 5314 (2010).
- ¹⁷ M. Wierzblick and R. Swirkowicz, *Phys. Rev. B* **84**, 075410 (2011).
- ¹⁸ P. Trocha and J. Barnas, *Phys. Rev. B* **85**, 085408 (2012).
- ¹⁹ K. P. Wojcik and I. Weymann, *Phys. Rev. B* **89**, 165303 (2014).
- ²⁰ C. C. Chen, David M T Kuo and Y. C. Chang, *Phys. Chem. Chem. Phys.* **17**, 19386 (2015).
- ²¹ M Galperin, A. Nitzan, and MA Ratner, *Molecular Physics* **106**, 397 (2008)
- ²² Yu-Sen Liu, and Y. Chang Chen, *Phys. Rev. B* **79**, 193101 (2009).
- ²³ J. Fransson and Galperin M, *Phys. Chem. Chem. Phys.* **13**, 14350 (2011).
- ²⁴ M. Esposito, M. A. Ochoa and M. Galperin, *Phys. Rev. B* **91**, 115417 (2015).
- ²⁵ C. C. Chen, Y. C. Chang and David M T Kuo, *Phys. Chem. Chem. Phys.* **17**, 6606 (2015).
- ²⁶ H. Haug and A. P. Jauho, *Quantum Kinetics in Transport and Optics of Semiconductors* (Springer, Heidelberg, 1996).
- ²⁷ A. P. Jauho, N. S. Wingreen and Y. Meir, *Phys. Rev. B* **50**, 5528 (1994), and references therein.
- ²⁸ B. R. Bulka and T. Kostyrko, *Phys. Rev. B* **70**, 205333 (2004).
- ²⁹ T. A. Costi and V. Zlati, *Phys. Rev. B* **81**, 235127 (2010).
- ³⁰ For details, see PhD thesis of Chih-Chieh Chen, University of Illinois at Urbana-Champaign (2015) available at <https://www.ideals.illinois.edu/handle/2142/88937>.
- ³¹ David M. T. Kuo and Y. C. Chang, *Nanotechnology*, **24**, 175403 (2013).
- ³² N. Nakpathomkun, H. Q. Xu and H. Linke, *Phys. Rev. B*

- 82**, 235428 (2010).
- ³³ M. Leijnse, M. R. Wegewijs and K. Flensberg, Phys. Rev. B **82**, 045412 (2010).
- ³⁴ Y. S. Liu, X. F. Yang, X. K. Hong, M. S. Si, F. Chi and Y. Guo. App. Phys. Lett, **103**, 093901 (2013).
- ³⁵ S. F. Svensson, E. A. Hoffmann, N. Nakpathomkun, P. M. Mu, H. Q. Xu, H. A. Nilsson, D. Sanchez, V. kashcheyevs and H. Linke, New. J. Phys. **15**, 105011 (2013).
- ³⁶ K. Grove-Rasmussen, H. I. Jorgensen, T. Hayashi, P. E. Lindelof, and T. Fujisawa, Nano Letters, **8** 1055 (2008).
- ³⁷ T. Kostyrko, Tomasz and B. R. Bulka, Phys. Rev. B **79** 075310 (2009).
- ³⁸ C. Y. Hsieh, Y. P. Shim, Yun-Pil, and P. Hawrylak, Phys. Rev. B **85** 085309 (2012).
- ³⁹ K. Wrzesniewski, and I. Weymann, Phys. Rev. B **92** 045407 (2015).
- ⁴⁰ A. I. Hochbaum, R. K. Chen, R. D. Delgado, W. J. Liang, E. C. Garnett, M. Najarian, A. Majumdar, and P. D. Yang, Nature **451**, 7175 (2008).
- ⁴¹ A. I. Boukai, Y. Bunimovich, J. Tahir-Kheli, J. K. Yu, W. A. Goddard, J. R. Heath, Nature **451**, 168 (2008).
- ⁴² Y. Zhang, M. S. Dresselhuas, Y. Shi, Z. Ren and G. Chen, Nano. Lett. **11**, 1166 (2011).
- ⁴³ H. Thierschmann, F. Arnold, M. Mittermuller, L. Maier, C. Heyn, W. Hansen, H. Buhmann and L. W Molenkamp, New. J. Phys. **17**, 113003 (2015).
- ⁴⁴ J. Zhu, K. Hippalgaonkar, S. Shen, KV Wang, Y. Abate, S. Lee, J. Wu, X. Yin, A. Majumdar and X. Zhang, Nano Lett, **14**, 4867 (2014).
- ⁴⁵ B. Sothmann, R. Sanchez and A. N. Jordan, Nanotechnology, **26**, 032001(2015).

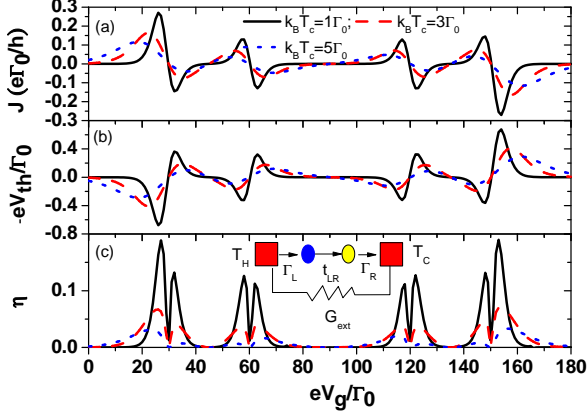


FIG. 1: Full many-body calculation results for (a) Electron current (J), (b) thermal voltage (eV_{th}/Γ_0) and (c) efficiency (η) of DQD as functions of gate voltage V_g ($E_\ell = E_0 = E_F + 30\Gamma_0 - eV_g$) for various values of T_C . To find the ratio of η to the Carnot efficiency, we should multiply η in (c) by a scaling factor $(T_C + \Delta T)/\Delta T$, which is 2, 4, and 6 for $k_B T_C = 1, 3$, and $5\Gamma_0$, respectively. We have used the following physical parameters $t_{LR} = 1\Gamma_0$, $U_\ell = 60\Gamma_0$, $U_{LR} = 30\Gamma_0$, and $\Gamma_L = \Gamma_R = \Gamma = 1\Gamma_0$. G_{ext} is set to $0.2G_0$.

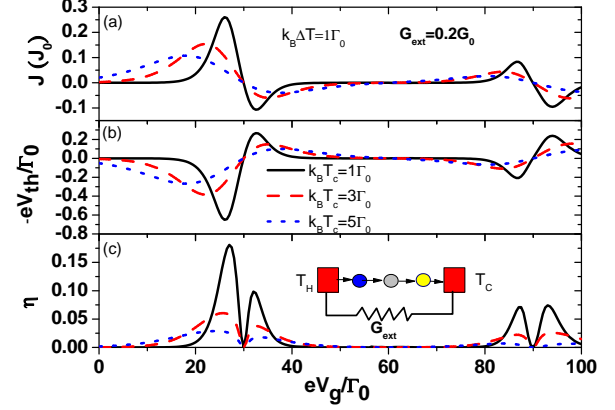


FIG. 3: Full many-body calculation results for (a) Electron current (J), (b) thermal voltage (eV_{th}) and (c) EHE efficiency (η) of SCTQD as functions of gate voltage V_g ($E_\ell = E_F + 30\Gamma_0 - eV_g$) in SCTQD for various values of T_C with $k_B \Delta T = 1\Gamma_0$. Other physical parameters are the same as those of Fig. 2. $G_{ext} = 0.2G_0$ and $Q_{ph} = 0$.

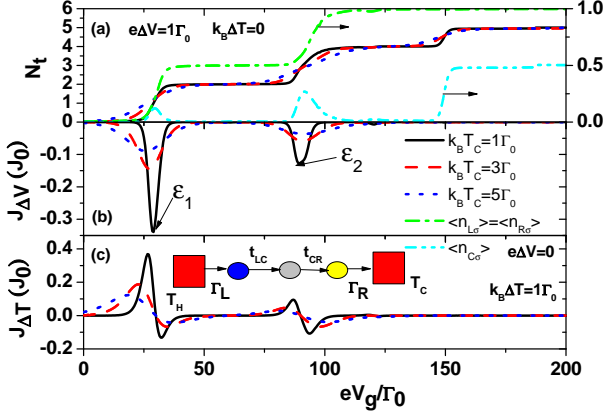


FIG. 2: Full many-body calculation results of SCTQD for (a) Total occupation number, (b) electron current ($J_{\Delta V}$) due to fixed electrical bias $e\Delta V = 1\Gamma_0$ and $k_B \Delta T = 0$, and (c) electron current ($J_{\Delta T}$) due to fixed temperature bias ΔT as functions of the gate voltage V_g ($E_\ell = E_0 = E_F + 30\Gamma_0 - eV_g$) for various values of T_C with $k_B \Delta T = 1\Gamma_0$ and $e\Delta V = 0$. We used the following physical parameters $t_{LC} = t_{CR} = 1\Gamma_0$, $t_{LR} = 0$, $U_\ell = 60\Gamma_0$, $U_{LC} = U_{CR} = 30\Gamma_0$, and $\Gamma_L = \Gamma_R = \Gamma = 1\Gamma_0$. $J_0 = e\Gamma_0/h$. Both R_{ext} and Q_{ph} are set to zero.

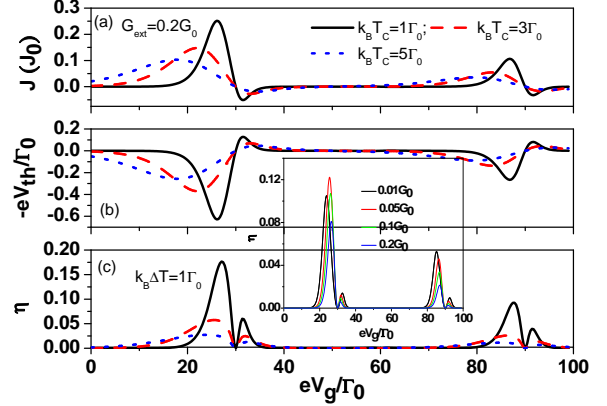


FIG. 4: Results obtained by method B for (a) Electron current (J), (b) thermal voltage (eV_{th}) and (c) EHE efficiency (η) of SCTQD as functions of gate voltage V_g ($E_\ell = E_F + 30\Gamma_0 - eV_g$) for various values of T_C with $k_B \Delta T = 1\Gamma_0$, $G_{ext} = 0.2G_0$, and $Q_{ph} = 0$. The inset of Fig. 4 shows the η including the effect of Q_{ph} for four G_{ext} values; 0.01, 0.05, 0.1 and $0.2G_0$ at $k_B T_C = 1\Gamma_0$.

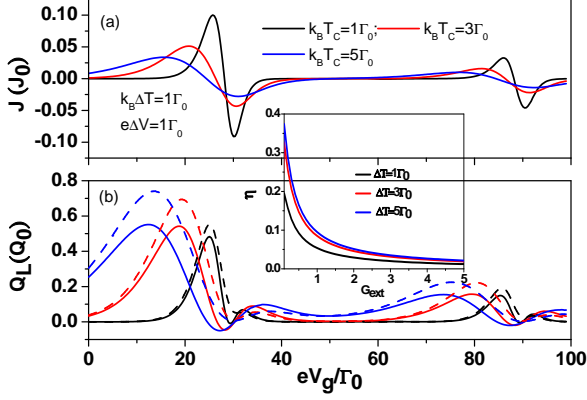


FIG. 5: Results obtained by method B for (a) electron current (J), and (b) heat current (Q_L in units of $Q_0 = \Gamma_0^2/h$) of SCTQD as functions of gate voltage V_g ($E_L = E_F + 30\Gamma_0 - eV_g$) for various values of T_C with $k_B\Delta T = 1\Gamma_0$. Solid curves are for ΔV fixed at $1\Gamma_0$, while the dashed curves in (b) are for a fixed load with $G_{ext} = 0.2G_0$. Other physical parameters are the same as those used for Fig. 4. The inset shows the η as functions of G_{ext} for different $k_B\Delta T$ values at $eV_g = 28\Gamma_0$ and $k_B T_C = 1\Gamma_0$.

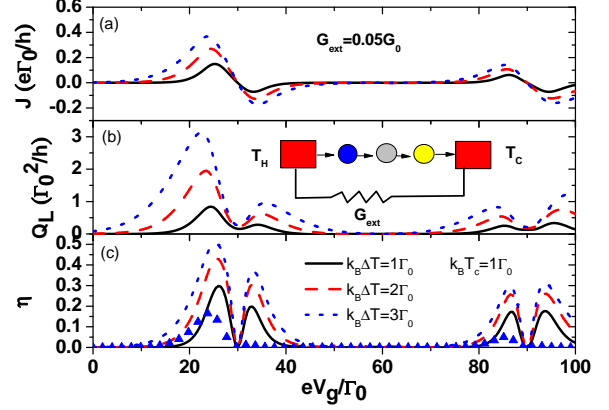


FIG. 7: (a) Electron current (J), (b) heat current (Q_L) and (c) EHE efficiency η as functions of QD energy level for different $k_B\Delta T$ values at $k_B T_C = 1\Gamma_0$ and $G_{ext} = 0.05G_0$. Other physical parameters are the same as those of Fig. 3. The curve with blue triangle marks shown in Fig. 7(c) is calculated by method B for the case of $k_B\Delta T = 3\Gamma_0$ to reveal the Q_{ph} effect. To find the ratio of η to the Carnot efficiency, we should multiply η in (c) by a scaling factor $(T_C + \Delta T)/\Delta T$, which is 2, 3, and 4 for $k_B T_C = 1, 2$, and $3\Gamma_0$, respectively.

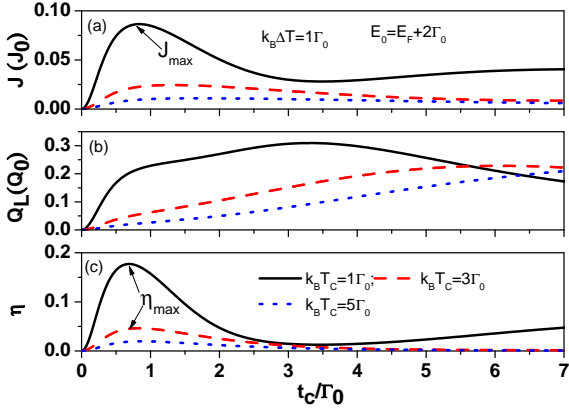


FIG. 6: Results obtained by method B for (a) electron current (J), (b) heat current (Q_L in units of $Q_0 = \Gamma_0^2/h$), and (c) EHE efficiency of SCTQD as functions of electron hopping strength $t_{LC} = t_{CR} = t_c$ for various values of T_C with $k_B\Delta T = 1\Gamma_0$. Other physical parameters are the same as those used for Fig. 5. To find the ratio of η to the Carnot efficiency, we should multiply η in (c) by a scaling factor $(T_C + \Delta T)/\Delta T$, which is 2, 4, and 6 for $k_B T_C = 1, 3$, and $5\Gamma_0$, respectively.

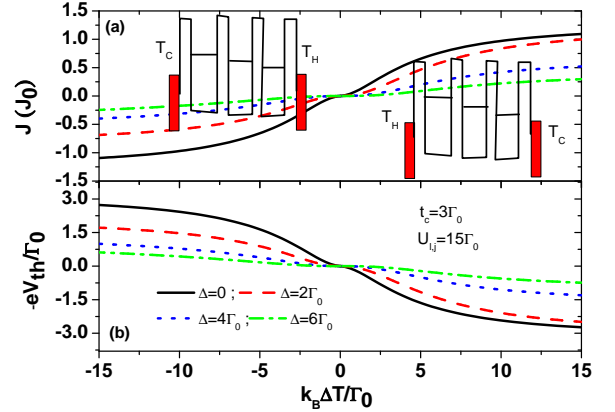


FIG. 8: (a) Electron current (J) and (b) thermal voltage (eV_{th}) as functions of temperature bias for different QDM configurations ($E_R = E_F + 10\Gamma_0$, $E_C = E_R + \Delta$, and $E_L = E_R + 2\Delta$) with $t_c = 3\Gamma_0$, $U_{l,j} = 15\Gamma_0$, and $k_B T_c = 1\Gamma_0$. We have considered QD energy levels shifted by V_{th} . Here $E_{L(R)}$ is replaced by $\epsilon_{L(R)} = E_{L(R)} \mp 0.3eV_{th}$. Other physical parameters are the same as those of Fig. 3.

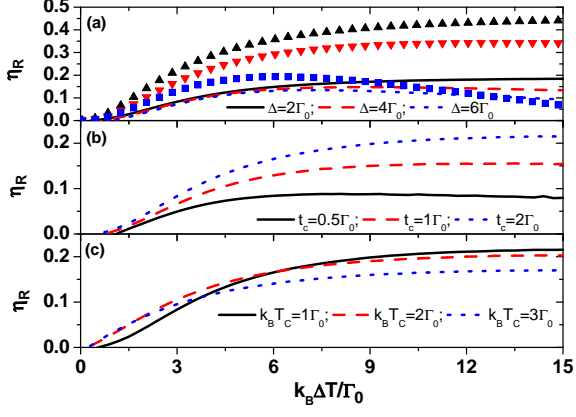


FIG. 9: Electron current rectification efficiency (η_R) as a function of temperature bias for the variation of different physical parameters. (a) Δ is varied, while $t_c = 3\Gamma_0$ and $k_B T_c = 1\Gamma_0$. (b) t_c is varied, while $\Delta = 2\Gamma_0$ and $k_B T_c = 1\Gamma_0$. (c) T_c is varied, while $\Delta = 2\Gamma_0$ and $t_c = 2\Gamma_0$. Other physical parameters are the same as those of Fig. 8.